DIFFERENCE ANALYSIS FOR FLUID-STRUCTURE INTERACTION

E. GIENCKE, M. FORKEL

Technische Universität Berlin, Lehrstuhl und Institut für Konstruktionslehre, Salzufer 17-19, D-1000 Berlin 10, Germany

Summary

For solving fluid structure interaction problems it is possible to organize the computer programs for the difference method in the same way as for the finite element method by establishing the difference equations with the principial of virtual work. In the finite element method the individual localized functions for the approximation of the potential function Φ will be chosen also as virtual functions $\delta\Phi$. Deriving difference equations the virtual states are simple as possible and the approximation of the potential function may be linear or parabolic. The equations become symmetric both for points in the interiour and at the boundaries and for grids with rectangular and triangular elements. The boundary and edge-conditions shall established for elastic walls and for the free surface. For regular rectangular and triangular grids it is possible to derive on the same way multipoint difference equations,which for the same numbers of unknwons are two orders better in accuracy as the usual difference or the finite element equations. Some examples for the pressure distribution in a BWR-steel-containment due to steam bubble collaps at the condenser pipes will be shown.

1. Introduction

Idealizing the fluid as an ideal incompressible fluid it is favourable to intruduce the potential functions Φ. For approximate solutions the differential equation $\Delta\Phi = 0$ may be substituted by the corresponding variational principle

$$\iint (\Phi_x \delta\Phi_x + \Phi_y \delta\Phi_y)\, dxdy - \int (\Phi_n \delta\Phi + \Phi\delta\Phi_n)\, ds = 0. \qquad (1)$$

Approximating the potential function by localized bilinear functions (in fig. 1b for a rectangular and in fig. 1c for triangular elements) in the variational methods the same bilinear functions have to chose as virtual states, because only the unknown values of Φ, the coefficients of the Ritz-power serious, have to variate. On this way we get the following equation for a regular rectangular grid with the x-distance h and the y-distance k (fig. 1b)

$$\begin{array}{|ccc|} \hline -1 & 2 & -1 \\ -4 & \boxed{8} & -4 \\ -1 & 2 & -1 \\ \hline \end{array} \frac{\Phi k}{6h} + \begin{array}{|ccc|} \hline -1 & -4 & -1 \\ 2 & \boxed{8} & 2 \\ -1 & -4 & -1 \\ \hline \end{array} \frac{\Phi k}{6h} = 0. \qquad (2)$$

In this scheme only the coefficients of the unknowns are given in the same spatial arrangement as the unknowns, the considered point is framed.

2. Difference equations

The same equations may be derived in a simpler way. To that we consider first a beam and establish the equilibrium equation between the moments M and the distributed load p by the principal of virtual displacement (fig. 1d). That is the virtual work of the moments M at the kinks $\delta\beta$ and the work of the load p at the virtual displacement δw/1/

$$\delta W = \sum M \delta\beta + \int p\delta\, w dx. \qquad (3)$$

Approximating the load linearly of parabolically from eq. (3) follows

$$\delta W = \begin{array}{|ccc|} \hline 1 & \boxed{-2} & 1 \\ \hline \end{array} \frac{M}{h} + \left\{ \begin{array}{|ccc|} \hline 1 & \boxed{4} & 1 \\ \hline \end{array} /6 \right\} ph = 0. \quad \text{lin.}$$

$$\left\{ \begin{array}{|ccc|} \hline 1 & \boxed{10} & 1 \\ \hline \end{array} /12 \right\} \quad \text{parab.} \quad \text{approx.} \qquad (3a)$$

If we introduce the same principle to fluids, then the potential function Φ works as bending moments at the "kinks" $\delta\phi_n$ (fig. 1e,f) and the normal derivative Φ_n as shearing forces at the "displacement" $\delta\Phi$ at the grid-lines (fig. 1f)

$$\delta W = \int (\Phi\delta\Phi_n + \Phi_n\delta\Phi)\, ds = 0. \qquad (4)$$

The last term is only needed at the boundaries, if Φ_n do not vanish there. We have to solve only line integrals instead of surface integrals in eq. (1). After approximating the potential function linearly from point to point we get in this way also eq. (2) for a rectangular grid.

If the potential function is approximated by parabolas about three

points as in fig. 1d (that are Lagragian polynoms) only the weighting coefficients change from |1 4 1|/ 6 to |1 1o 1|/12

$$\begin{bmatrix} -1 & 2 & -1 \\ -1o & \boxed{2o} & -1o \\ -1 & 2 & -1 \end{bmatrix} \frac{\Phi k}{12h} + \begin{bmatrix} -1 & -1o & -1 \\ 2 & \boxed{2o} & 2 \\ -1 & -1o & -1 \end{bmatrix} \frac{\Phi h}{12K} = 0. \qquad (5)$$

For the integration of the parabolic potential function with the triangular virtual kink $\delta\Phi_n$ we obtain the operator 1 1o 1 /12. The second order difference 1 -2 1 in the other direction of the difference scheme results automatically, because the kink $\delta\Phi_n$ on the center line in fig. 1e is twice as large and opposite to those on the outer lines. Eq. (5) becomes two orders more accurate than eq. (2), it is the multipoint difference equation for the potential function /1/. In accuracy it is the best equation for the chosen influence zone, including the considered point and the surrounding points only, because the parabola is the best approach for the potential function by using only three support points in each direction.

For triangular elements the analysis becomes very simple, because the virtual kinks are constant along each gridline. For a single triangular element we get with the virtual kinks $\delta\Phi_n$ in fig. 1f the virtual work

$$\delta W = (x_{23}\, x_{ij} + y_{23}\, y_{ij})\, \Phi_k / F_{123} \quad [ijk \text{ cyclical } 1,2,3]. \qquad (6)$$

That is the same operator as for plates and shells in the formulation of /2/. The equations (2), (5), (6) are symmetric both in the interiour and at the boundaries. The computerprograms may be organized to establish the equations pointwise or elementwise.

At a symmetry-line only the half operator (2) or (5) and at an edge point only the quarter are to use. At elastic walls the virtual work in the elastic walls must be added. At an elastic wall the fluid velocity Φ_n normal to the wall and the velocity of the wall deflection w must agree [$(\,)^{\cdot}$ is the time derivative]

$$\Phi_n = \dot{w}. \qquad (7)$$

The pressure p at the wall may be expressed by the potential function

$$p = -\rho\dot{\Phi} \qquad (8a)$$

and by the differential equation of the shell (the relationship between the load and the deformation). If only the essential circumferential membrane stiffness is considered and the inertia forces in the shell are omitted (allowable for steel containments), this equations becomes for a cylindrical shell (thickness t, radius r, Youngs modulus E) very simple

$$p = \frac{Et}{r^2} w \qquad (8b)$$

or finally with eq. (7) and (8a)

$$p = -\rho\dot{\Phi} = \frac{Et}{r^2} \Phi_x. \qquad (9)$$

Using the principle of virtual work, the corresponding virtual work

$$\int \phi_x \delta\phi \, dy = -\int \frac{\rho r^2}{Et} \phi \delta\phi ds, \tag{10}$$

which usually cancel itselve at interiour points, must be added. Thus we get for an linear approach of the potential function the difference equation

$$\begin{bmatrix} -1 & 1 \\ -4 & \boxed{4} \\ -1 & 1 \end{bmatrix} \frac{\Phi k}{6h} + \begin{bmatrix} -1 & -2 \\ 2 & \boxed{4} \\ -1 & -2 \end{bmatrix} \frac{\Phi h}{6k} + \begin{bmatrix} 1 \\ \boxed{4} \\ 1 \end{bmatrix} \frac{\rho r^2}{Et} \frac{\ddot{\Phi} k}{6h} = 0 \tag{11}$$

for a point at the right hand elastic wall. Analysing the eigenvalues ω and modes

$$\ddot{\underline{\Phi}} = -\omega^2 \underline{\Phi}.$$

3. Example

The influence of the wall elasticity in a suppression system of a BWR reactor (fig. 2a) on the pressure distribution due to steam bubble collaps at the condenser pipes shall discussed. If at each condenser pipe the same pressure time history $p_o(t)$ occurs, a small cylindrical sector only must be investigated instead of the whole containment (fig. 2b). Because of the small angle of the sector-cell it may be substituted by a rectangular cell of the same volume (fig. 2b) and we get only a two dimensional problem. The difference between the results for a rectangular and a circular sector cell appears only for a collaps at the excentric pipe 1, for a collaps at the centric pipes 2 and 3 it is within the drawing accuracy in fig. 2b. Further more the cross-section of the containment will be simplified by substituting the outer spherical shell within the water zone by a cylindrical shell and the conical bottom by a flat bottom (fig. 2a). The analysis will be done in two steps: First the pressure distribution in the stiff containment and then in the elastic one. Thus we are able to show directly how the pressure peaks are reduced by the wall-elasticity.

3.1 Stiff containment

The pressure distribution in some distance from the bubble can be described by the well known source-solution $\phi(x,y,z)$ /3/

$$p(x,y,z,t) = -\rho\dot{\Phi}(x,y,z,t) = p(t)\phi(x,y,z). \tag{12}$$

Because of the singularity of the source solution at the source point it is favourable to introduce the solution for an infinite containment as basic solution. In order to approach already the effect of the walls and the bottom source and sinks may be arranged in a regular pattern (fig. 2c). To simulate the walls and the free surface the sources must be arranged symmetrically to the walls and antimetrically to the free surface (fig. 2c). The convergence of the solution will be better if on a vertical line the numbers of sources and sinks are the same /4/. The additional potential function ϕ solved numerically by difference equations, have only to fulfil the boundary

conditions at the walls and at the free surfaces

$$\text{wall: } \Phi_n = \phi_{n,o} + \phi_n = 0 \qquad \text{free surface: } \Phi = \phi_o + \phi = 0 \tag{13}$$

The computer program for elastic and stiff walls is the same. The boundary condition at the free surface can be approached by $\Phi = 0$, because the inertial forces due to the sloshing of the free fluid surface are small.

3.2 Elastic containment

To involve wall elasticity first the modes $f_n(x,y)$ of the fluid-containment-system must be derived and then the pressure distribution in the stiff containment must be represented by a power serious in the modes (fig. 4b)

$$p(x,y,t) = \sum p_k(t)\ f_n(x,y) \tag{14}$$

and finally the dynamical response of each mode must be calculated and superimposed to the resulting pressure /5/. We get exact solutions and are able to compare the numerical and the analytical ones, if the connection between the walls and the bottom is neglected and only the membrane stiffness of the walls in circumferential direction is considered (8b).

For a container with a stiff interiour wall and bottom (fig. 3a) we get the modes in fig. 3b. They are sinefunctions in vertical direction and hyperbolic-cosine-functions in horizontal direction. In fig. 3b also the solution of the multipoint difference method is shown as dashed line. By using only one element with two unknowns, it agrees very well to the exact solution (solid line). To get the same accuracy by linear approximation of Φ the height and the width have to devided fourfold. The additional influence of the interiour wall-elasticity, which are because of the smaller curvature more stiff than the outer wall, is investigated in fig. 4. In this case two modes in horizontal direction are yield for each sinefunction (in vertical direction), one from the elasticity of the outer wall (λ_1) and the other from the elasticity of the interiour wall (λ_2). The modes decrease from the walls into the interiour of the fluid, from the interiour wall much more than from the elastic outer one and further more with increasing order n of the modes. Thus at the higher modes only the fluid in the immediate surrounding of the walls moves and the remaining fluid in the containment rests. Before solving the eigenvalue problem the potential function in the interiour points can be eliminated by boundary values, because the eigenvalue ω is only contained in the boundary equation (11) at elastic walls. Thus the eigenvalue problem only includes the boundary values of the potential function as nodes.

To improve the convergence of the power serious (14) for the pressure it is important to seperate the solution for the stiff containment and to calculate it directly as in fig. 2 and not by a power serious. In fig. 5 the maximum pressure distribution along the walls is drawn for two cells (I and II). Following cells will be considered: $2o^o$-cell (I) with two pipes 3 and one pipe 1 and 2 and a $1o^o$-cell (II) with the pipes 2 and 3. The dashed dotted lines are the results for a stiff containment and the solid lines are

the results in an elastic containment. Due to the elasticity the pressure decreases approximately to the half. Further the pressure distribution at the more elastic outer wall is more even as at the stiffer interiour wall. The pressure bulges there results from the excentric pipe 1. In addition some pressure time histories will be shown in fig. 5: The time history at a pipe (p_o) and in the edges between the walls and the bottom. The pressure at the walls oscillate essentially with the lowest frequence of that wall. The frequency of the interiour wall is two times higher than that of the outer wall. The maximum pressure at the interiour wall is larger as at the more elastic outer wall.

4. References

/1/ Giencke, E.: The Mechanical Interpretation of High Accuracy Multipoint Difference Methods for Plates and Shells, IUTAM Symp. High Speed Computing of Elastic Structures, Liège, 1971. Les Congrés et Colloques de Université de Liège. Vol. 61 (1971).

/2/ Giencke, E.: A Simple Mixed Method for Plate and Shell Problems. Nuclear Engineering and Design 29 (1974), 141-155.

/3/ Lamb, H.: Hydrodynamics. Dover Publ. New York, 1945.

/4/ Giencke, E., Forkel, M: The Pressure Distribution Due to a Steam Bubble Collaps in a Stiff Containment. March 1978 (Interiour Report - will be published as ILR-Report).

/5/ Giencke, E.: The Influence of the Wall-Elasticity on the Pressure Distribution in a Suppression Chamber of the KKK. Jule 1978 (Interiour Report).

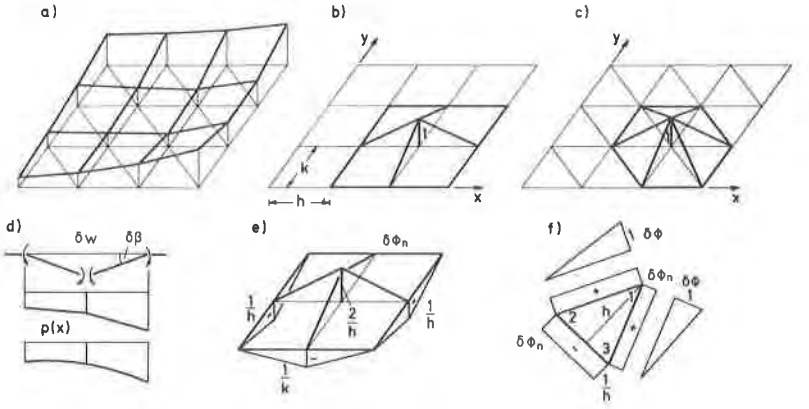

Fig. 1: Real and virtual states for the potential function Φ

a) Linear approximation,

b) Localized function for rectangular, c) for triangular elements,

d) Beam problem (virt. displacement δw, lin. and parab. approx. for the load)

e) concentrated virtual state for rectangular and f) for triangular elements

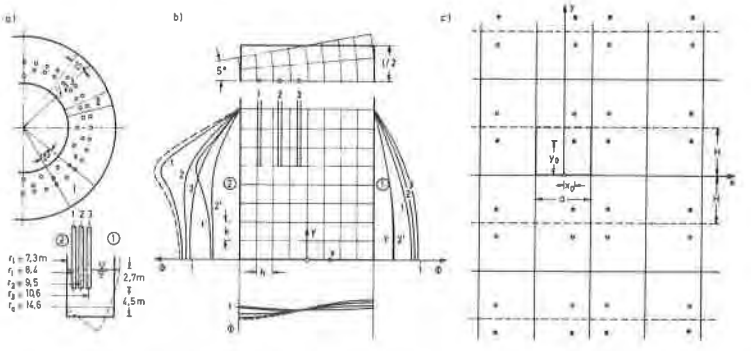

Fig. 2: Pressure distribution due to steam bubble collaps in a stiff containment

a) Container (-- original, — idealized crossection)

b) Pressure distribution due to a collaps at different condenser pipes: 1,2,3 in 10^{o}-cell, 1'2' in 20^{o}-cell (— rectangular cell, -- sector cell)

c) Arrangement of the sources for the basic solution Φ_o (● source, o sink)

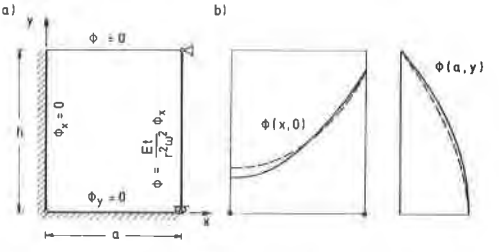

Fig. 3: First mode for a containment with a stiff interiour wall and bottom

a) System, b) Grid and results (— exact, -- multipoint difference solution)

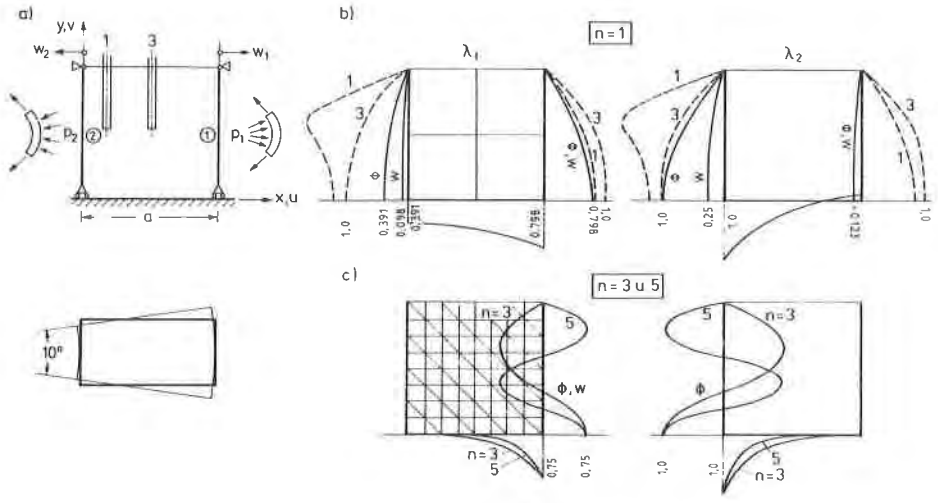

Fig. 4: Modes for a containment with stiff bottom and elastic walls
a) System, b) First modes for the potential function Φ and the wall deflection w, rectangular grid
(— modes, -- pressure distribution in the stiff containment)
c) Higher modes and triangular grid

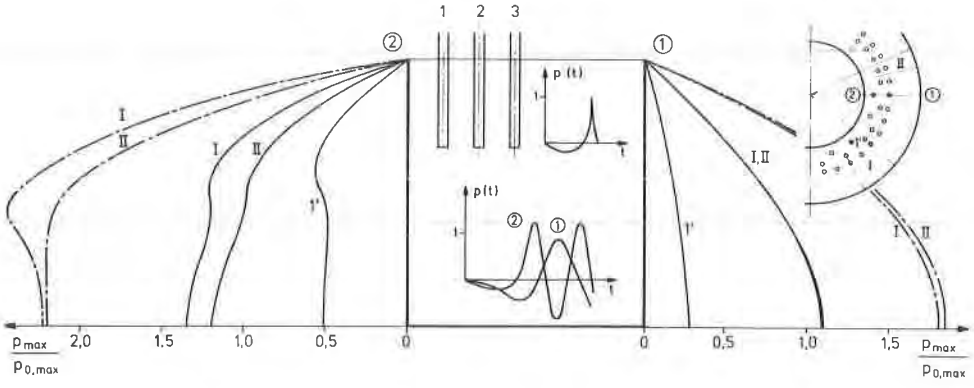

Fig. 5: Maximum pressure distribution along the walls due to a simultaneous steam bubble collaps in three combinations
1' : collaps at pipe 1 in a 20°-cell
I : collaps at pipe 1,2 and at two pipes 3 in a 20°-cell
II : collaps at the pipes 2,3 in a 10°-cell
(— elastical, -.- stiff containment)